INTERNATIONAL JOURNAL FOR NUMERICAL METHODS IN ENGINEERING
*Int. J. Numer. Meth. Engng* 2007; **69**:504–523
Published online 5 June 2006 in Wiley InterScience (www.interscience.wiley.com). DOI: 10.1002/nme.1778

# 1-Norm-based regularization scheme for system identification of structures with discontinuous system parameters

Hyun Woo Park[1, ‡], Man Woo Park[2, 3, §, ¶], Byeong Kyu Ahn[3, 4, ¶, ‖] and Hae Sung Lee[5, *, †, **]

[1]*Korea Bridge Design and Engineering Research Center, Seoul National University, Seoul 151-742, Korea*
[2]*Structure Department, DONG IL Engineering Consultants Co. Ltd., Seoul 138-200, Korea*
[3]*Department of Civil Engineering, Seoul National University, Korea*
[4]*Structural Design Department, Korea Engineering Consultants Corp., Seoul 143-715, Korea*
[5]*School of Civil, Urban, and Geosystem Engineering, Seoul National University, Seoul 151-742, Korea*

SUMMARY

This paper presents a new class of regularization functions and the associated regularization scheme for structural system identification. In particular, 1-norm regularization functions are investigated to overcome the smearing effect of 2-norm regularization functions for the identification of discontinuous system parameters of structures. The truncated singular value decomposition is employed to filter out noise-polluted solution components and to impose the 1-norm regularization function on SI. The bilinear fitting method is proposed for selecting an optimal truncation number of the truncated singular value decomposition. The validity of the proposed method is demonstrated through the identification of an inclusion in a square plate and damaged members in a two-span truss. Copyright © 2006 John Wiley & Sons, Ltd.

Received 9 June 2005; Revised 1 April 2006; Accepted 17 April 2006

KEY WORDS: regularization scheme; 1-norm regularization function; 2-norm regularization function; system identification; optimal truncation number; bilinear fitting method

*Correspondence to: Hae Sung Lee, School of Civil, Urban, and Geosystem Engineering, Seoul National University, San 56-1, Shillim-dong, Kwanak-gu, Seoul 151-742, Korea.
†E-mail: chslee@plaza.snu.ac.kr
‡Senior Research Associate.
§Assistant Engineer.
¶Former Graduate Student.
‖Assistant Manager.
**Associate Professor.

Contract/grant sponsor: Korea Research Foundation; contract/grant number: KRF-2000-013-EA0136

## 1. INTRODUCTION

Various system identification (SI) algorithms have been proposed during the last few decades to estimate material properties of structural systems [1–5]. Most of the SI algorithms are based on minimizing an error function consisting of least-squares errors between measured and calculated responses of a structure. The calculated responses are obtained through the structural analysis using the numerical model of a structure. In general, SI suffers from ill-posedness of an inverse problem due to the sparseness and the noise of measured data [5–12], which cause the non-uniqueness and/or discontinuity of solutions [5–9]. Unless the ill-posedness of SI is properly addressed, SI algorithms rarely yield numerically stable and physically meaningful solutions [5–12].

To alleviate the ill-posedness of SI, a regularization technique has been widely employed [5–9]. In the regularization technique, a regularization function defining a proper solution space of a system parameter is imposed on the minimization problem of an SI algorithm [6, 9]. Here, a system parameter implies the material or stiffness property of a structure to be estimated through SI. The regularization scheme using a 2-norm regularization function is frequently adopted in various SI problems [9, 13, 14], and is referred to as the 2-norm-based regularization scheme. The 2-norm-based regularization schemes effectively stabilize the ill-posedness of SI [5, 7–9, 11, 12]. However, they usually produce smeared solutions due to smoothing characteristics of 2-norm minimization in case the actual distribution of the system parameter is discontinuous in a structural domain [9]. The smearing effect of the 2-norm-based regularization schemes has been reported in edge detection of image reconstruction problems. The total variational [15] and the piecewise polynomial truncated singular value decomposition [16] have been proposed to overcome the smearing effect of the 2-norm regularization function. However, little attention has been paid to addressing this problem in SI of structural systems.

This paper presents a new class of regularization functions for SI of continuous and framed structures with discontinuous system parameters. The proposed regularization function is defined by the 1-norm of a system parameter vector, and the regularization scheme using the 1-norm regularization function is referred to as the 1-norm-based regularization scheme hereafter. Since material properties of a continuous structure are square integrable, the solution space for a material property is defined by the $L_1$-norm of the gradient of the material property. The 1-norm regularization function for a continuous structure is obtained by discretizing the $L_1$-norm defining the solution space. The 1-norm regularization function for a framed structure is directly defined by the 1-norm of the cross-sectional rigidities of members as they are given independently for each member in a discrete fashion.

Since the 1-norm of a vector is not differentiable, the Newton-type solution scheme, which requires the gradient information of an object function, is not suitable for the SI with the 1-norm regularization function. The truncated singular value decomposition (TSVD) is adopted to minimize the error function with the 1-norm regularization function. Two optimization problems are defined in the TSVD. The first optimization problem calculates the solution components of a quadratic sub-problem of the error function that are not affected by measurement noise by truncating solution components corresponding to smaller singular values. The 1-norm regularization function is used to restore the truncated solution components in the second optimization, which is performed by the simplex method for each quadratic sub-problem of the error function. A truncation number in the TSVD plays a crucial role in SI since the truncation number controls the stability and accuracy of the solution. The bilinear fitting method (BFM) is proposed in this paper to determine an optimal truncation number. The proposed BFM is also applicable to 2-norm-based regularization schemes.



DOI: 10.1002/nme

The validity of the proposed method is demonstrated through reconstructing discontinuous Young's modulus of a square plate with an inclusion and axial rigidities of members in a two-span truss with damage. It is shown that the proposed 1-norm-based regularization scheme effectively prevents the information of a system parameter from smearing out, and thus accurately reconstructs discontinuous system parameters in a structural domain.

## 2. 1-NORM REGULARIZATION FUNCTIONS

### *2.1. Error function and instability of SI problems*

The displacement field of a structure under the static condition is calculated by a stiffness equation, which is derived by using the finite element method (FEM) or similar discretization methods.

$$\mathbf{K}(\mathbf{D})\mathbf{u}_i = \mathbf{P}_i \quad \text{for } i = 1, \ldots, nlc \tag{1}$$

where $\mathbf{D}$, $\mathbf{K}$, $\mathbf{u}_i$, $\mathbf{P}_i$, and $nlc$ are the discretized system parameter vector, the stiffness matrix, the nodal displacement vector of the structure, nodal load vector for load case $i$, and the number of load cases, respectively. The system parameters of a structure may include material properties, displacement boundary conditions, geometry, etc. In this paper, it is assumed that either the material or stiffness properties of the structure are the only unknown system parameters to be identified, and that the exact loading conditions are given.

The system parameters of a structure are identified through a SI procedure by minimizing least-squares errors between measured and calculated displacements at observation points under the known loading conditions [5, 7, 8].

$$\underset{\mathbf{D}}{\text{Min}}\ \Pi_E = \frac{1}{2}\sum_{i=1}^{nlc} \|\tilde{\mathbf{u}}_i(\mathbf{D}) - \bar{\mathbf{u}}_i\|_2^2 \quad \text{subject to } \mathbf{R}(\mathbf{D}) \leqslant 0 \tag{2}$$

where $\tilde{\mathbf{u}}_i$, $\bar{\mathbf{u}}_i$ and $\mathbf{R}$ are the calculated displacement vector by the numerical model (1), the measured displacement vector at observation points for load case $i$, and a constraint vector for the system parameter vector, respectively, while $\|\cdot\|_2$ denotes the 2-norm of a vector. The constraint is specified for setting the upper and lower bound of the system parameter vector for physical significance, and expressed by a linear form [5, 8].

$$\mathbf{D}_l \leqslant \mathbf{D} \leqslant \mathbf{D}_u \tag{3}$$

Here $\mathbf{D}_l$ and $\mathbf{D}_u$ represent the lower and upper bounds of the system parameters, respectively.

The SI problem defined by the minimization problem (2) is a type of inverse problem that suffers from ill-posedness. The ill-posedness of inverse problems is characterized by the discontinuity and non-uniqueness of solutions, which are caused by noises in measurements and the sparseness of measured data. Unless these instabilities of the SI problems are addressed properly, the solution procedures of the SI problems become numerically unstable, and exhibit extremely slow convergence or divergence [5, 7, 8]. Even if a converged solution is obtained, the solution is likely to be physically meaningless.

To alleviate the instabilities of SI problems, a regularization technique, which has been widely used in many inverse problems, is adopted in this study. In the regularization technique, a proper solution space for the SI problem is defined by a regularization function, which has to be incorporated into the minimization problem (2). In the following subsections, a new class of regularization



DOI: 10.1002/nme

functions is proposed to define proper solution spaces for the material properties of a continuous structure and the cross-sectional rigidities of members of a framed structure.

### 2.2. *Discretized 1-norm regularization function for a continuous structure*

A numerically stable and physically meaningful solution of (2) is obtained by specifying a proper solution space, which is defined by the norm of the system parameter. In many inverse problems in engineering fields, *a priori* information on the system parameter is available based on engineering sense or previous experiences. The *a priori* information, which includes the smoothness of a solution and an initial estimate of a solution, is used to define the regularization function. The initial estimate of a solution is hereafter referred to as a baseline solution.

A material property of a continuous structure may vary in piecewise-continuous fashion, and thus has to be square integrable in the structural domain. Should an actual solution exist within the sphere of radius $a$ centred at the baseline solution in a square integrable function space, the solution space is defined by the following $L_2$-norm [13, 14].

$$\Psi_2(D) = \|D - D_0\|^2_{L_2(V)} = \int_V (D - D_0)^2 \, \mathrm{d}V \leqslant a^2 < \infty \tag{4}$$

where $\Psi$, $D$, $D_0$ and $\|\cdot\|_{L_2(V)}$ are the regularization function, a material property, the baseline solution for the material property and the $L_2$-norm of a function defined in a structural domain $V$, respectively. The subscript of $\Psi$ indicates the order of the norm used in the regularization function.

To discretize a material property of a continuous structure, the structural domain is divided into a finite number of sub-domains as shown in Figure 1. The discretized material property is assumed constant in a sub-domain, which may consist of a finite element or a predefined group of finite elements. The discretized form of (4) is expressed as

$$\Psi_2 = \int_V (D - D_0)^2 \, \mathrm{d}V \approx \sum_{e=1}^{ng} (D^e - D_0^e)^2 A^e = \|\mathbf{L}_2^c(\mathbf{D} - \mathbf{D}_0)\|_2^2 \tag{5}$$

where $ng$, $D^e$, and $D_0^e$ represent the number of sub-domains, the material property and its baseline solution of sub-domain $e$, respectively. Each component of $\mathbf{D}$ and $\mathbf{D}_0$ corresponds to the discretized material property to be estimated and its baseline solution of each sub-domain, respectively. $\mathbf{L}_2^c$ is

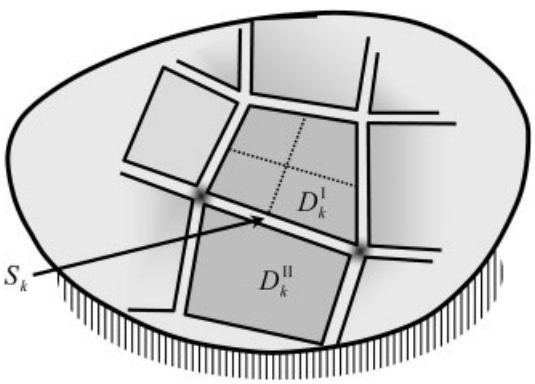


Figure 1. Discretization of a domain with predefined groups and inter-group boundaries.



DOI: 10.1002/nme

a diagonal weighting matrix that has diagonal entries equal to the square roots of the areas of the element groups.

The regularization function (5) has been commonly used in a 2-norm-based regularization scheme for the identification of piecewise continuous system parameters [5–9, 12]. The Tikhonov regularization technique and the conventional truncated singular value decomposition are typical 2-norm-based regularization schemes. Though the 2-norm-based regularization schemes effectively stabilize ill-posedness of SI, they often produce blurry solutions [9], in which information on the system parameter of a group is smeared into that of other groups. Therefore, the regularization schemes based on the 2-norm of the system parameter vector are not suitable for reconstructing the discontinuous distribution of system parameters accurately.

The solution space for a square integrable system parameter around the baseline solution is alternatively defined by the $L_1$-norm of the gradient of the system parameter as follows:

$$\Psi_1(D) = \|\nabla(D - D_0)\|_{L_1(V)} = \int_V \|\nabla(D - D_0)\|_1 \, \mathrm{d}V \leqslant a < \infty \tag{6}$$

where $\nabla$, $\|\cdot\|_{L_1(V)}$ and $\|\cdot\|_1$ are the gradient operator, the $L_1$-norm of a function defined in a structural domain $V$ and the 1-norm of a vector, respectively. To integrate the $L_1$-norm of the gradient of the material property in a domain discretized by sub-domains, consider a domain with two sub-domains as shown in Figure 2. It is assumed that the material property is constant in each sub-domain. The two sub-domains and their interface boundary are denoted as $V_1$, $V_2$ and $S$, respectively, in Figure 2. A narrow transition region of width $2\varepsilon$ along boundary $S$ is considered to integrate (6). The material property in the transition region is assumed to vary linearly in the normal direction of $S$, and to be constant in the tangential direction of $S$, which leads to the

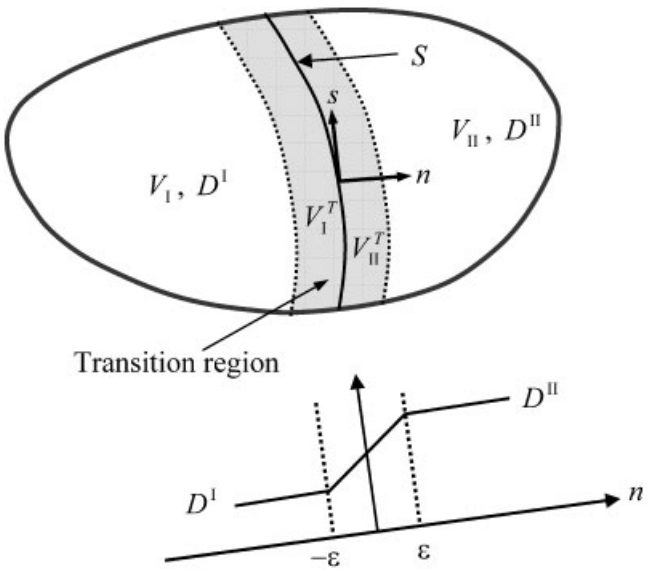


Figure 2. Transition region along the interface boundary between two sub-domains.



DOI: 10.1002/nme

following expression:

$$D(n,s)=\frac{D^{\mathrm{II}}-D^{\mathrm{I}}}{2\varepsilon}n+\frac{D^{\mathrm{II}}+D^{\mathrm{I}}}{2} \tag{7}$$

where $D^{\mathrm{I}}$ and $D^{\mathrm{II}}$ represent the discretized material property of sub-domain I and II, respectively. For simplicity of presentation, $D_0$ is omitted during the discretization procedure. The $L_1$-norm given in (6) is discretized as follows:

$$\begin{aligned}\int_V \|\nabla D\|_1\,\mathrm{d}V &= \int_V \left(\left|\frac{\partial D}{\partial x}\right|+\left|\frac{\partial D}{\partial y}\right|\right)\mathrm{d}V\\ &= \lim_{\varepsilon\to 0}\left(\int_{V_{\mathrm{I}}-V_{\mathrm{I}}^{\mathrm{T}}}\left(\left|\frac{\partial D}{\partial x}\right|+\left|\frac{\partial D}{\partial y}\right|\right)\mathrm{d}V+\int_{V_{\mathrm{II}}-V_{\mathrm{II}}^{\mathrm{T}}}\left(\left|\frac{\partial D}{\partial x}\right|+\left|\frac{\partial D}{\partial y}\right|\right)\mathrm{d}V\right.\\ &\quad\left.+\int_{V_{\mathrm{I}}^{\mathrm{T}}+V_{\mathrm{II}}^{\mathrm{T}}}\left(\left|\frac{\partial D}{\partial x}\right|+\left|\frac{\partial D}{\partial y}\right|\right)\mathrm{d}V\right)\end{aligned} \tag{8}$$

where $V_{\mathrm{I}}^{\mathrm{T}}$ and $V_{\mathrm{II}}^{\mathrm{T}}$ are the transition region in sub-domain I and II, respectively. The derivatives of the material property in the transition region are expressed in terms of the directional derivatives of $n$ and $s$ direction.

$$\begin{aligned}\frac{\partial D}{\partial x}&=\frac{\partial D}{\partial n}\cos\theta+\frac{\partial D}{\partial s}\sin\theta=\frac{D^{\mathrm{II}}-D^{\mathrm{I}}}{2\varepsilon}\cos\theta\\ \frac{\partial D}{\partial y}&=-\frac{\partial D}{\partial n}\sin\theta+\frac{\partial D}{\partial s}\cos\theta=-\frac{D^{\mathrm{II}}-D^{\mathrm{I}}}{2\varepsilon}\sin\theta\end{aligned} \tag{9}$$

where $\theta$ denotes the angle between the normal vector of $S$ and $x$-axis. Since the material property is assumed constant in each sub-domain in this study, the first two volume integrals in (8) vanish. The last integral of (8) is performed in the $n$–$s$ coordinate system of the transition region using (9).

$$\begin{aligned}\int_V \|\nabla D\|_1\,\mathrm{d}V &= \lim_{\varepsilon\to 0}\int_{V_{\mathrm{I}}^{\mathrm{T}}+V_{\mathrm{II}}^{\mathrm{T}}}\left(\left|\frac{\partial D}{\partial x}\right|+\left|\frac{\partial D}{\partial y}\right|\right)\mathrm{d}V\\ &= \lim_{\varepsilon\to 0}\int_0^l\int_{-\varepsilon}^{\varepsilon}\left(\left|\frac{D^{\mathrm{II}}-D^{\mathrm{I}}}{2\varepsilon}\cos\theta\right|+\left|\frac{D^{\mathrm{II}}-D^{\mathrm{I}}}{2\varepsilon}\sin\theta\right|\right)\mathrm{d}n\,\mathrm{d}s\\ &= \lim_{\varepsilon\to 0}\int_0^l\left(\left|\frac{D^{\mathrm{II}}-D^{\mathrm{I}}}{2\varepsilon}\cos\theta\right|+\left|\frac{D^{\mathrm{II}}-D^{\mathrm{I}}}{2\varepsilon}\sin\theta\right|\right)2\varepsilon\,\mathrm{d}s\\ &= |D^{\mathrm{II}}-D^{\mathrm{I}}|\int_0^l(|\cos\theta|+|\sin\theta|)\,\mathrm{d}s\\ &= |D^{\mathrm{II}}-D^{\mathrm{I}}|(l_x+l_y)\end{aligned} \tag{10}$$

where $l_x$ and $l_y$ are the projected length of the interface boundary onto $x$- and $y$-axis, respectively.



DOI: 10.1002/nme

In case the domain of the body is discretized into several sub-domains as shown in Figure 1, the regularization function in (6) is discretized by using (10) as follows:

$$\int_V \|\nabla(D - D_0)\|_1 \, \mathrm{d}V \approx \sum_{k=1}^{n_B} |(D_k^{\mathrm{I}} - (D_k^{\mathrm{I}})_0) - (D_k^{\mathrm{II}} - (D_k^{\mathrm{II}})_0)|((l_k)_x + (l_k)_y) \tag{11}$$

where $n_B$ and $l_k$ denote the number of inter-group boundaries and the length of the $k$th inter-group boundary, respectively, while $(l_k)_x$ and $(l_k)_y$ represent the projected lengths of the $k$th inter-group boundary onto $x$- and $y$-axis, respectively. $D_k^{\mathrm{I}}$, $D_k^{\mathrm{II}}$, $(D_k^{\mathrm{I}})_0$ and $(D_k^{\mathrm{II}})_0$ represent the material properties to be identified and the associated baseline solutions of two groups sharing the $k$th inter-group boundary $S_k$ as shown in Figure 1. The discretized regularization function (11) is expressed with a discrete derivative operator $\mathbf{L}_1^c$.

$$\sum_{k=1}^{n_B} \left| (D_k^{\mathrm{I}} - (D_k^{\mathrm{I}})_0) - (D_k^{\mathrm{II}} - (D_k^{\mathrm{II}})_0) \right| ((l_k)_x + (l_k)_y) = \left\| \mathbf{L}_1^c (\mathbf{D} - \mathbf{D}_0) \right\|_1 \tag{12}$$

The discrete derivative operator $\mathbf{L}_1^c$ is determined based on the group connectivity and the geometry of groups.

### *2.3. 1-norm regularization function for a framed structure*

The stiffness property of a framed structure is represented by cross-sectional rigidities, which are independently defined for each member as follows [17]:

$$D^e = \int_{A^e} f(A) \, \mathrm{d}A \tag{13}$$

where $D^e$ and $A^e$ are the cross-sectional rigidity and the cross-sectional area of member $e$ in a framed structure, respectively, and $f(A)$ is a function of the cross-sectional and the material property. For example, the axial rigidity and the flexural rigidity with respect to $z'$-axis of each member are obtained by taking $f(A) = E$ and $f(A) = E(y')^2$, respectively. Here, $E$ is Young's modulus while $y'$ and $z'$ are the local $y$- and $z$-axis of each member, respectively, as shown in Figure 3. It is assumed that a cross-sectional rigidity is constant in each member.

Once the cross-sectional rigidity of each member is independently defined in a discrete fashion, the cross-sectional rigidities are discretely distributed in a given structural domain. In this case, the solution space of (2) is given by a vector norm rather than a function norm used for a continuous

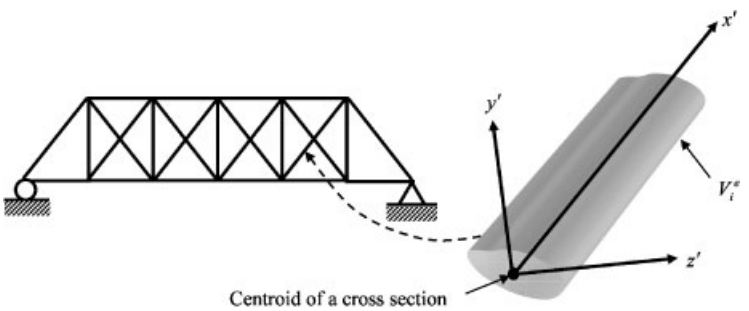


Figure 3. Local axes of member $e$ and the idealization of a framed structure.



DOI: 10.1002/nme

structure in (4). The solution space for the cross-sectional rigidity of each member is often defined by the 2-norm as follows:

$$\Psi_2 = \|\mathbf{D} - \mathbf{D}_0\|_2^2 = \sum_e (D^e - D_0^e)^2 \leqslant a^2 < \infty \tag{14}$$

As described in the previous section, the 2-norm regularization function yields blurry identification results. To avoid the smearing effect and to reconstruct the discretely distributed cross-sectional rigidities of members in a framed structure accurately, the 1-norm of the system parameter vector is employed as the regularization function. The solution space of (2) defined by the 1-norm is given for a framed structure as follows:

$$\Psi_1 = \|\mathbf{D} - \mathbf{D}_0\|_1 = \sum_e |D^e - D_0^e| \leqslant a < \infty \tag{15}$$

It should be noted that the regularization function in (15) is obtained by substituting the discrete derivative operator $\mathbf{L}_1^c$ in (12) with an identity matrix. This is because the cross-sectional rigidities of a framed structure are defined independently and discretely for each member.

## 3. OPTIMIZATION

### *3.1. 1-norm-based regularization scheme with the TSVD*

A proper regularization function for a given problem is imposed to the original minimization problem (2) by regularization techniques. The Tikhonov regularization technique [5–9, 12] and the TSVD [11, 18] are widely used. In the Tikhonov regularization technique, the regularization function is added to the original error function (2), and the optimization is performed for the regularized error function as follows:

$$\underset{\mathbf{D}}{\text{Min}}\ \Pi = \frac{1}{2}\|\widetilde{\mathbf{U}}(\mathbf{D}) - \overline{\mathbf{U}}\|_2^2 + \frac{\lambda}{2}\Psi \quad \text{subject to} \quad \mathbf{R}(\mathbf{D}) \leqslant 0 \tag{16}$$

where $\Psi$ represents a proper regularization function defined in the previous section, and $\lambda$ is the regularization factor, which controls the degree of regularization [5, 11, 12]. $\widetilde{\mathbf{U}}$ and $\overline{\mathbf{U}}$ are vectors obtained by arranging the vectors of the computed displacements and the measured displacements for each load case in a row, respectively. Because the minimization problem (16) is nonlinear with respect to the system parameter vector, an iterative solution scheme should be employed. However, a Newton-type algorithm, which requires the gradient information of $\Psi$, cannot be applied to solve (16) in case the regularization function is defined by the non-differentiable 1-norm of the system parameter vector.

This paper utilizes the TSVD to impose the 1-norm regularization function iteratively in the optimization of the error function. In the TSVD, the incremental solution of the error function is obtained by solving quadratic sub-problems without constraints, and then the noise-polluted solution components are truncated from the incremental solution. Finally, the optimization of the regularization function is performed to restore truncated solution components and constraints. The above procedure is defined as follows:

$$\underset{\mathbf{D}}{\text{Min}}\ \Psi = \|\mathbf{L}(\mathbf{D} - \mathbf{D}_0)\|_1 \quad \text{subject to} \quad \mathbf{R}(\mathbf{D}) \leqslant 0 \quad \text{and} \quad \underset{\mathbf{D}}{\text{Min}}\ \Pi_E = \frac{1}{2}\|\widetilde{\mathbf{U}}(\mathbf{D}) - \overline{\mathbf{U}}\|_2^2 \tag{17}$$

The weighting matrix $\mathbf{L} = \mathbf{L}_1^c$ for a continuous structure, and $\mathbf{L} = \mathbf{I}$ for a framed structure.



DOI: 10.1002/nme

The incremental solution for the minimization of the error function is obtained by solving the following quadratic sub-problem [5]:

$$\underset{\Delta\mathbf{D}}{\text{Min}} \|\mathbf{S}\Delta\mathbf{D} - \mathbf{U}_{k-1}^{r}\|_2^2 \tag{18}$$

where $\Delta\mathbf{D}$, and $\mathbf{S}$ are the solution increment and the sensitivity matrix of the displacement fields with respect to the system parameters at the observation points, respectively, and the subscript $k$ denotes the iteration count. The displacement residual $\mathbf{U}_{k-1}^{r}$ is defined as $\mathbf{U}_{k-1}^{r} = \overline{\mathbf{U}} - \widetilde{\mathbf{U}}_{k-1}$, where $\widetilde{\mathbf{U}}_{k-1}$ is the displacement field calculated by the converged system parameters at the previous iteration.

The first-order necessary optimality condition for (18) is given as the following linear equation:

$$\mathbf{S}^{\mathrm{T}}\mathbf{S}\Delta\mathbf{D} - \mathbf{S}^{\mathrm{T}}\mathbf{U}_{k-1}^{r} = 0 \tag{19}$$

The solution of (19) is obtained by the singular value decomposition of the sensitivity matrix as follows [11, 18]:

$$\Delta\mathbf{D} = \sum_{j=1}^{p} \frac{\mathbf{z}_j^{\mathrm{T}}\mathbf{U}^{r}}{\omega_j}\mathbf{v}_j + \sum_{j=p+1}^{n} \gamma_j \mathbf{v}_j \tag{20}$$

where $\mathbf{z}_j$ and $\mathbf{v}_j$ are the left singular vector (LSV) and the right singular vector (RSV) of the sensitivity matrix, respectively, and $\omega_j$ is the $j$th singular value of $\mathbf{S}$ which has the descending order of $\omega_{\max} = \omega_1 \geqslant \omega_2 \geqslant \cdots \geqslant \omega_n = \omega_{\min} \geqslant 0$. The RSVs are the basis vectors for the incremental solution of the quadratic sub-problem. In (20), $n$ and $p$ denote the number of unknown system parameters and the rank of the sensitivity matrix, respectively, and the coefficients $\gamma_j$ represent undetermined constants for rank-deficient cases, i.e. $p<n$. In the case of $p \geqslant n$, no undetermined constant is defined in (20), and the solution of (19) is given only by the first term of (20). When $\omega_1 \gg \omega_p$, the SI problem is considered to be a discrete ill-posed one [11]. Since a finite number of significant digits are used in real calculations, the rank of the sensitivity matrix is determined by the numerical rank [18].

The solution given in (20) satisfies (19) for all real $\gamma_j$ in rank-deficient problems, which causes the non-uniqueness of solutions. The regularization function provides additional information to define the undetermined constants $\gamma_j$. The solution components corresponding to the smaller singular values are responsible for the discontinuity of the solution because noise components amplified by small singular values pollute a whole solution [5]. To obtain stable solutions, the noise-polluted solution components should be removed from (20) by truncating the solution components associated with the singular values smaller than a critical singular value $\omega_t$ $(t \leqslant p)$. Here, $t$ is a truncation number, which plays the crucial role of filtering out noise-polluted components in the incremental solution (20) [11]. An algorithm to determine the optimal truncation number is presented in the next section.

The truncated components of the incremental solution in (20) are replaced with a linear combination of the truncated RSVs, which increases the number of the undetermined constants.

$$\Delta\mathbf{D} = \sum_{j=1}^{t} \frac{\mathbf{z}_j^{\mathrm{T}}\mathbf{U}^{r}}{\omega_j}\mathbf{v}_j + \sum_{j=t+1}^{n} \gamma_j \mathbf{v}_j = \Delta\mathbf{D}_t + \mathbf{q} \tag{21}$$



DOI: 10.1002/nme

where

$$\Delta \mathbf{D}_t = \sum_{j=1}^{t} \frac{\mathbf{z}_j^{\mathrm{T}} \mathbf{U}^r}{\omega_j} \mathbf{v}_j, \quad \mathbf{q} = \sum_{j=t+1}^{n} \gamma_j \mathbf{v}_j \tag{22}$$

The incremental form of (17) is expressed with respect to $\mathbf{q}$ as follows:

$$\begin{aligned} &\underset{\mathbf{q}}{\mathrm{Min}} \quad \|\mathbf{L}(\mathbf{q} - (\mathbf{D}_0 - \mathbf{D}_{k-1} - \Delta \mathbf{D}_t))\|_1 \\ &\text{subject to} \quad \mathbf{V}_t^{\mathrm{T}} \mathbf{q} = 0 \quad \text{and} \quad \mathbf{D}_l - \mathbf{D}_{k-1} - \Delta \mathbf{D}_t \leqslant \mathbf{q} \leqslant \mathbf{D}_u - \mathbf{D}_{k-1} - \Delta \mathbf{D}_t \end{aligned} \tag{23}$$

where $\mathbf{V}_t = (\mathbf{v}_1, \mathbf{v}_2, \ldots, \mathbf{v}_t)$. The equality constraint of (23) represents that $\mathbf{q}$ should be a linear combination of the truncated RSVs. The optimization problem defined in (23) is a linear programming with respect to $\mathbf{q}$, and is solved by the simplex method [19]. Once the optimal solution of (23) is obtained from the linear programming, a line search is performed for the error function to accelerate convergence.

Since the 1-norm optimization in (23) yields a limited number of non-zero solution components depending on the truncation number, the 1-norm-based regularization function effectively reduces the smearing effect often observed in the 2-norm-based regularization scheme. Detailed discussions on this issue can be found in Reference [16].

### *3.2. Bilinear fitting method*

It is crucial to determine a proper truncation number so that the TSVD produces a numerically stable and physically meaningful solution. The truncation number plays a similar role to the regularization factor in the Tikhonov regularization technique. In case a truncation number is too small, most of the useful information on a structure is lost while too large a truncation number yields noise-polluted, meaningless solutions [11, 20]. Therefore, the truncation number should be determined so that useful information of a structure is retained as much as possible while noise-polluted solution components are truncated.

The optimal truncation number may be defined as the truncation number associated with the smallest singular value that does not amplify noise in measurement. The bilinear fitting method (BFM) is proposed to determine the optimal truncation number for the TSVD in this paper. The truncation number for (23) is fixed throughout iterations in the BFM. Figure 4 illustrates schematically the variation of the residual of the error function with truncation numbers. As the truncation number approaches an optimal truncation number, the residual of the converged error function decreases very quickly since the number of useful solution components without amplified noise included in (21) increases. Once the truncation number becomes larger than the optimal truncation number, the decreasing rate of the error function suddenly reduces because noise-polluted solution components associated with smaller singular values are included in the first term of (21). Based on this observation, the plot of the residuals of the error function versus the truncation number is represented by two straight lines, i.e. a bilinear function as shown in Figure 4.

The bilinear function with the breaking point at the $i$th truncation number is defined as follows:

$$\begin{aligned} y_1^i(\tau) &= a_1^i(\tau - i) + c^i, \quad 1 \leqslant \tau \leqslant i \\ y_2^i(\tau) &= a_2^i(\tau - i) + c^i, \quad i \leqslant \tau \leqslant p \end{aligned} \tag{24}$$



DOI: 10.1002/nme

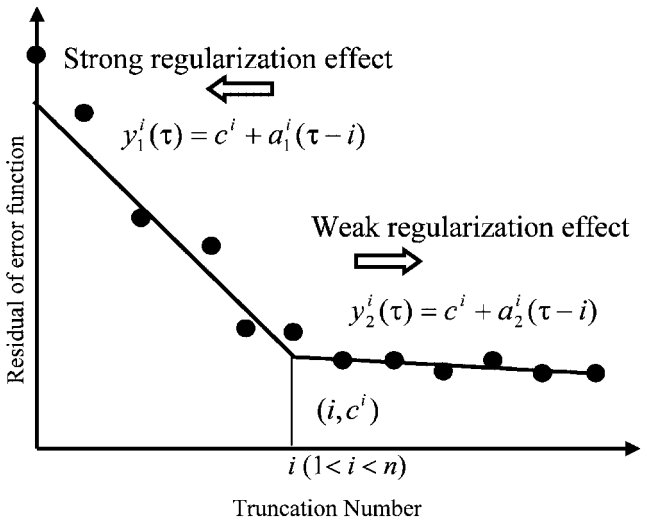


Figure 4. A schematic illustration of the bilinear fitting method.

where $\tau$ denotes a truncation number, and $a_1^i$, $a_2^i$, $c^i$ are the unknown coefficients of the bilinear function. The line segment with a steep slope denoted as $y_1^i(\tau)$ represents a region of strong regularization effect, while the line segment with a gentle slope denoted as $y_2^i(\tau)$ represents a region of week regularization effect. The coefficients $a_1^i$, $a_2^i$, $c^i$ in (24) are determined by the least-squares method as follows:

$$\underset{(a_1^i, a_2^i, c^i)}{\text{Min}} \ \pi^i = \sum_{k=1}^{i} (y_1^i(k) - \Pi_E^k)^2 + \sum_{k=i}^{p} (y_2^i(k) - \Pi_E^k)^2 \tag{25}$$

where $\Pi_E^k$ is the converged residual of the error function for truncation number $k$. The bilinear function is determined for each breaking point $1 \leqslant i \leqslant p$ by (25), and then the least-squares error between each best-fitting bilinear function and the residuals of the error function is evaluated.

$$\hat{\pi}^i = \sum_{k=1}^{i} (y_1^i(k) - \Pi_E^k)^2 + \sum_{k=i}^{p} (y_2^i(k) - \Pi_E^k)^2 \tag{26}$$

The breaking point of the bilinear function that minimizes (26) is chosen as an optimal truncation number, which yields the best trade-off between the regularization effect and the minimization of the error function. The bilinear function formed by the optimal truncation number represents the best-fit for the residual of the converged error function for each truncation number.

The proposed BFM can also be applied to 2-norm-based regularization schemes to determine an optimal regularization factor or truncation number. Since the only difference between 1- and 2-norm-based regularization schemes is the type of the regularization function, the proposed BFM is applicable to the 2-norm-based regularization scheme with a simple modification. For example, the procedure is modified slightly for the Tikhonov regularization scheme because the regularization factor instead of the truncation number controls the regularization effect. The BFM procedure



DOI: 10.1002/nme

is applied to the residuals of the error function computed by taking each singular value as the regularization factor.

## 4. NUMERICAL EXAMPLES

Numerical simulation studies are performed by the proposed method to identify inclusions in a square plate and damaged members in a two-span truss. The identification results obtained by the proposed method are compared to those by the TSVD with the 2-norm regularization function. For brevity of description, the TSVD with the 1- and 2-norm are referred to as the 1- and the 2-norm TSVD, respectively. The solution procedures of the 2-norm TSVD are exactly the same as those of the 1-norm TSVD described in Section 3.1 except for (23). To solve (23), the 2-norm TSVD adopts the sequential quadratic programming [21] instead of the simplex method used in the 1-norm TSVD. The optimal truncation numbers for the 1- and 2-norm TSVD are determined by the BFM. Proportional random noise generated by a uniform probability function between $\pm 5\%$ noise amplitude is added to the displacement fields obtained by numerical models to simulate real measurements in all cases.

### *4.1. Identification of inclusions in a square plate*

The proposed method is applied for the identification of a square inclusion and a pear-shaped inclusion in an 1 m $\times$ 1 m plate under the plane stress condition as shown in Figure 5. The geometry, boundary conditions and mesh layout for this example are illustrated in Figure 5. The material properties of the matrix plate are representative of steel ($E = 210$ GPa, $v = 0.3$), while the material properties of aluminium ($E = 70$ GPa, $v = 0.34$) are used for the inclusions. For the both examples, the area ratio of the inclusion to the whole plate is 6.3%, and the stiffness reduction ratio due to the presence of the aluminium inclusion is calculated as 4.2% of the steel plate without the inclusion.

The plate is discretized by 64 Q8 elements and 225 nodes for SI, which is shown in Figure 5. Each element forms a predefined element group, and the Young's modulus of each element is selected as the material property to be estimated. The Poisson ratio is fixed at its baseline solution, $v = 0.3$. Uniform tensions of 144 MPa are applied in $x$ and $y$ direction independently on the exterior boundaries of the plate. All components of displacement are measured for each load case at 32 equally spaced observation points, which are marked by solid circles in Figure 5. The Young's modulus of steel is taken as the baseline solution for each element.

*4.1.1. Identification of a square inclusion.* A square inclusion is identified in this example. The length of each side of the inclusion is 25 cm, and the centre of the inclusion is off centred from that of the plate (20.83 cm, 20.83 cm). The boundary of the inclusion does not coincide with finite element boundaries in the mesh layout used for SI. A fine mesh layout of 576 elements and 1825 nodes, in which the boundary of the inclusion coincides with the mesh boundary, is utilized to generate measured displacements at the observation points.

Figure 6 shows the residuals of the error function and the best fitting bilinear function corresponding to the optimal truncation number for the 1-norm TSVD. In the figure, the least-squares errors between the bilinear functions with different breaking points and the residuals of the error function are also plotted for the right vertical axis. Only 48 singular values out of 64 are used



DOI: 10.1002/nme

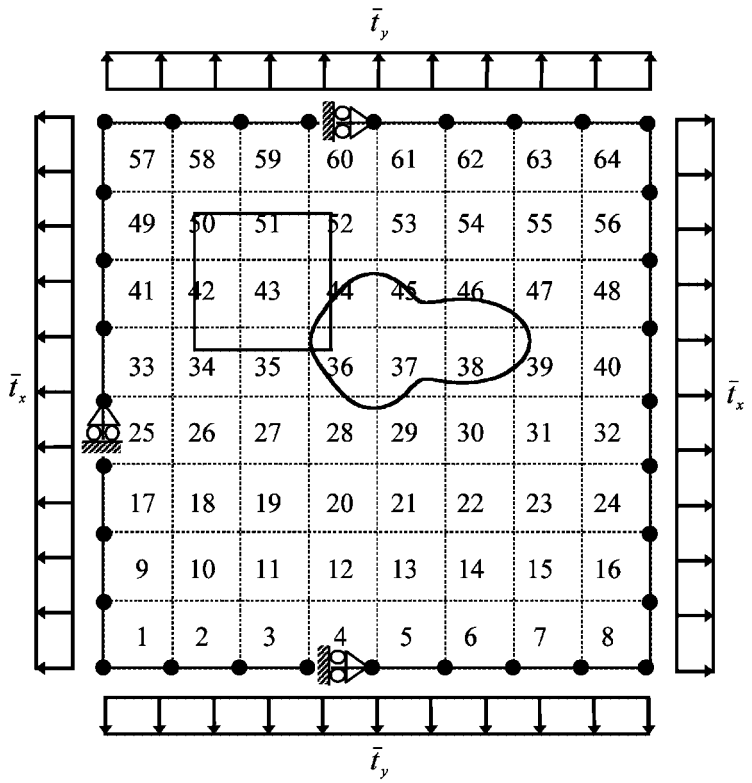


Figure 5. Mesh layout, boundaries conditions, observation points and inclusions of a square plate.

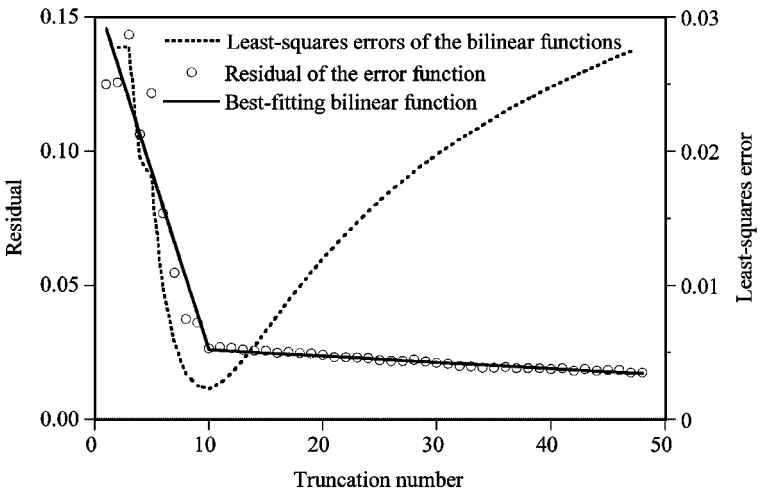


Figure 6. BFM for the identification of a square inclusion in a square plate.



DOI: 10.1002/nme

for the BFM since the simplex algorithm cannot find a solution of (23) for a truncation number greater than 48. The optimal truncation number is determined as 10. The best fitting bilinear function corresponding to the optimal truncation number well represents the variation of the residual of the error function with the truncation number. The optimal truncation number for the 2-norm TSVD is 8 by the BFM.

The identified Young's modulus of each element by the 1- and 2-norm TSVD is shown in Figure 7. The 2-norm TSVD produces more oscillating and inaccurate results than 1-norm TSVD. The 1-norm TSVD reconstructs the Young's moduli of most elements fixed near the baseline value, while the Young's moduli of the nine elements (element 34, 35, 36, 42, 43, 44, 50, 51, 52) are reduced prominently. The identified nine elements by the 1-norm TSVD encompass the actual inclusion as shown in Figure 8. There are two groups in the identified nine elements: the group of element 42, 43, 50 and 51 and the group of element 34, 35, 36, 44 and 52. The former group, which is darkly shaded in Figure 8, contains most of the inclusion, and the Young's moduli of these elements are reduced to 97.4 GPa. The latter group, which is lightly shaded in Figure 8, includes only a small portion of the inclusion, and thus the Young's modulus decreases to 147 GPa for element 34, 35, 36 and to 137 GPa for element 44, 52.

*4.1.2. Pear-shaped inclusion.* This example is presented by Lee *et al.* [7] for the identification of the geometric shape of the interface curve and the material properties of the inclusion using the boundary element method. The interface curve is generated by the following formula in a polar coordinate system:

$$r = \sqrt{\frac{(20 \times 10)^2}{(10\cos\theta)^2 + (20\sin\theta)^2}} + 3\cos 3\theta \tag{27}$$

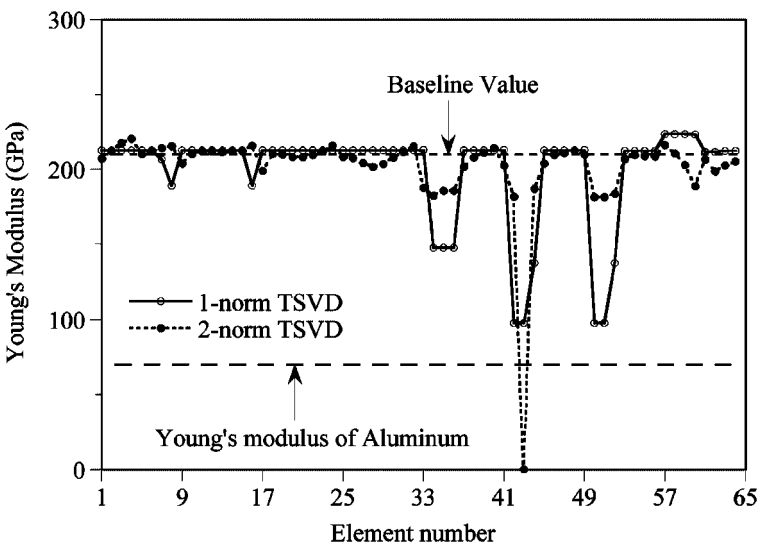


Figure 7. Identified Young's modulus of each group for the square inclusion.



DOI: 10.1002/nme

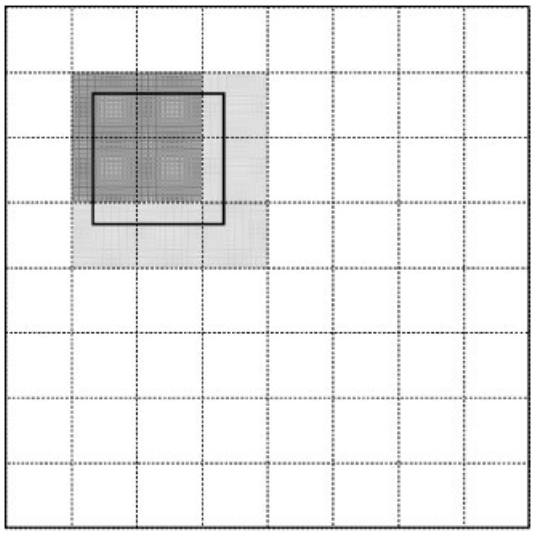

Figure 8. Identified groups for the square inclusion.

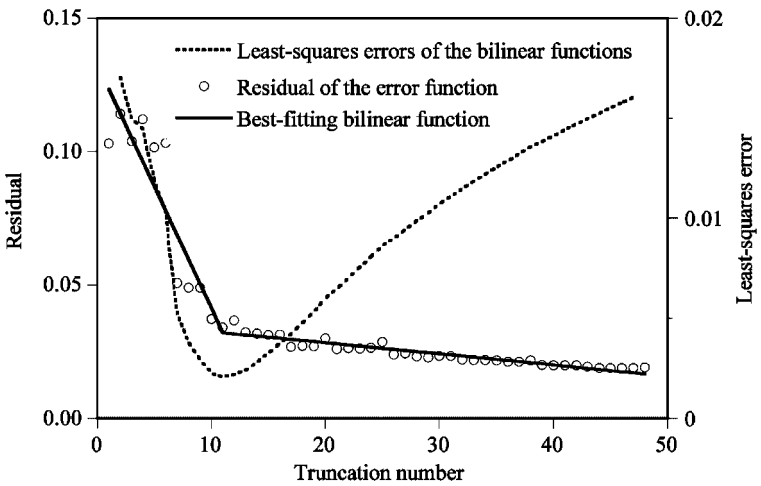


Figure 9. BFM for the identification of a pear-shaped inclusion in a square plate.

The measured data at the observation points are obtained by a boundary element model, which contains 256 quadratic elements on the exterior boundary and 128 quadratic elements on the interface between the inclusion and the matrix plate.

Figure 9 shows the residuals of the error function and the best fitting bilinear function corresponding to the optimal truncation number for the 1-norm TSVD. In the same figure, the least-squares errors between the bilinear functions with different breaking points and the residuals of the error



DOI: 10.1002/nme

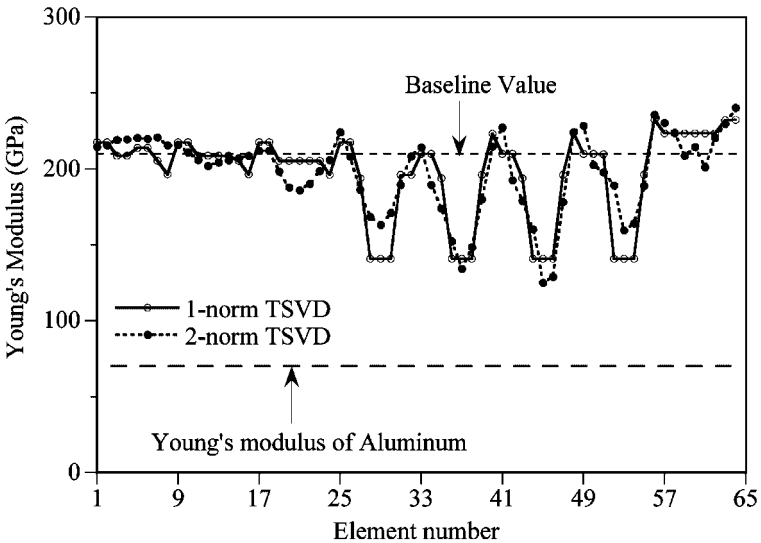


Figure 10. Identified Young's modulus of each group for the pear-shaped inclusion.

function are also plotted for the right vertical axis. Only 48 singular values out of 64 are used for the BFM as in the previous example. In this case, the optimal truncation number is determined as 11 for both the 1- and 2-norm TSVD.

Figure 10 illustrates the identified Young's modulus of each element by the 1- and 2-norm TSVD. The smearing effect of the 2-norm regularization function is clearly observed in the identified results by the 2-norm TSVD in the figure. The Young's moduli of most elements are fixed near the baseline value in case the 1-norm TSVD is adopted. The Young's moduli of the 12 elements (element 28, 29, 30, 36, 37, 38, 44, 45, 46, 52, 53, 54) are reduced prominently. The identified nine elements by the 1-norm TSVD encompass the actual inclusion as shown in Figure 11. Unlike the previous example, the identified 12 elements have the same Young's modulus regardless of the portion of the inclusion contained in each element.

### *4.2. Two-span truss*

Damaged members in a two-span truss shown in Figure 12 are identified in this example. Damage is simulated with 70 and 30% reduction in the axial rigidities of two bottom members (members 16 and 21), respectively. The axial rigidity of each member is taken as the material property to be estimated through the proposed method. The undamaged value of the axial rigidity of each member is assumed known *a priori*, and is used as the baseline solution. Figure 12 shows the geometry, support conditions and the locations of 12 observation points, which are depicted as solid circles in the figure. Horizontal displacements are measured at the roller supports and vertical displacements are measured at the other observation points independently for each load case shown in Figure 12. The BFM is performed for the first 30 singular values. The optimal truncation numbers for the 1- and 2-norm TSVD are selected as 4 and 3, respectively. The residuals of the error function and the best-fitting bilinear function corresponding to the optimal truncation number for the 1-norm TSVD are illustrated in Figure 13.



DOI: 10.1002/nme

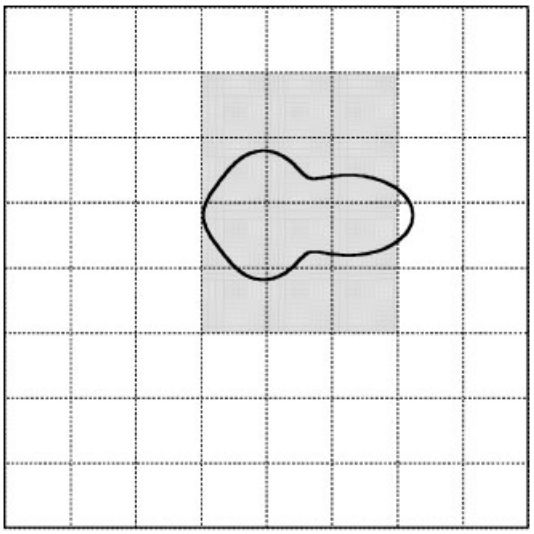

Figure 11. Identified groups for the pear-shaped inclusion.

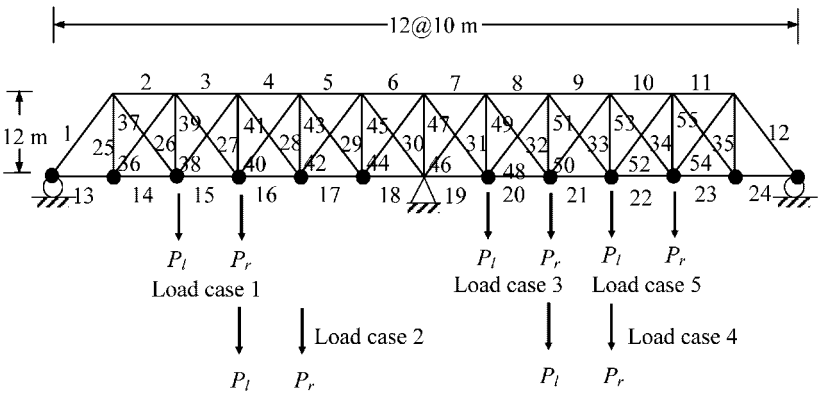


| Member | Area($cm^2$) | Member | Area($cm^2$) |
|---|---|---|---|
| Top | 250 | Vertical | 200 |
| Bottom | 300 | Diagonal | 220 |

Figure 12. Member ID numbers and load cases of the two-span truss.

Figure 14 shows the Young's modulus of each member identified by the 1- and 2-norm TSVD. The identified axial rigidities are normalized by the corresponding baseline solutions. The 1-norm TSVD yields sharp drops of the axial rigidities only at the damaged members, while the axial rigidities of the undamaged members are fixed near the baseline solutions. The 2-norm TSVD



DOI: 10.1002/nme

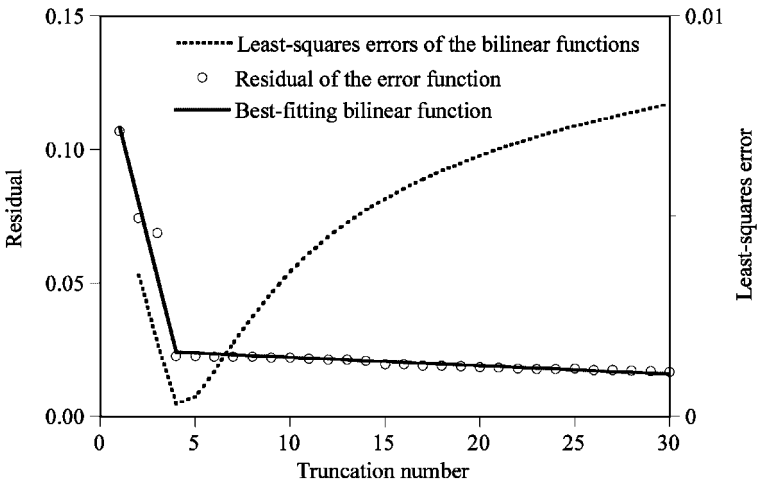


Figure 13. BFM for the isolation of damaged members in the two-span truss.

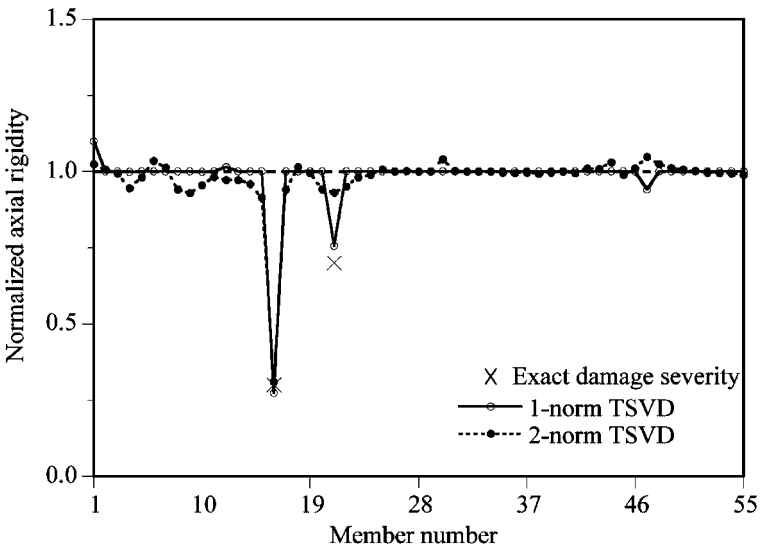


Figure 14. Identified axial rigidity of each member for the two-span truss.

yields more oscillating results than the 1-norm TSVD in upper and lower members. Although the damage in member 16 is clearly identified, most of the damage information of member 21 is smeared into members 20 and 22 in the 2-norm TSVD.

## 5. CONCLUSIONS

A new regularization scheme based on the 1-norm of a system parameter vector is proposed for system identification of continuous and framed structures. The 1-norm regularization function is



DOI: 10.1002/nme

imposed to define the solution space of an SI problem on the minimization of the error function, which is defined as the least-squares errors between calculated and measured displacements. The TSVD is utilized for filtering out noise components in a solution and restoring the truncated solution components by the optimization of the 1-norm regularization function, in which the simplex method is adopted. The BFM is proposed to select the optimal truncation number for the TSVD. The BFM is also applicable to the 2-norm-based regularization schemes for the determination of the optimal regularization factor or truncation number.

The proposed method is applied to the identification of inclusions with different material property in a square steel plate and to the isolation of damaged members in a two-span truss with numerically simulated measurements. In the square plate problem, the numerical model used in SI and the measured responses contain considerable modeling errors and random noise, respectively. Nevertheless, the proposed method identifies the inclusions successfully by restoring the discontinuities in Young's modulus of the plate. In the two-span truss problem, the damaged truss members are successfully localized by the proposed method without the smearing effect. It is concluded that the proposed method is capable of restoring discontinuous system parameters of structures accurately as well as alleviating the ill-posedness of SI problems effectively.

## ACKNOWLEDGEMENTS

The work was supported by the Korea Research Foundation Grant KRF-2000-013-EA0136.

## REFERENCES

1. Gioda G, Maier G. Direct search solution of an inverse problem in elastoplasticity: identification of cohesion, friction angle and in situ stress by pressure tunnel test. *International Journal for Numerical Methods in Engineering* 1980; **15**:1823–1848.
2. Norris MA, Meirovitch L. On the problem of modeling for parameter identification in distributed structures. *International Journal for Numerical Methods in Engineering* 1989; **28**:2451–2463.
3. Honjo Y, Wen-Tsung L, Guha S. Inverse analysis of an embankment on soft clay by extended Bayesian method. *International Journal for Numerical and Analytical Methods in Geomechanics* 1994; **18**:709–734.
4. Mahnken R, Stein E. Parameter identification for viscoplastic models based on analytical derivatives of a least-squares functional and stability investigations. *International Journal of Plasticity* 1996; **12**(4):451–479.
5. Park HW, Shin SB, Lee HS. Determination of an optimal regularization factor in system identification with Tikhonov function for linear elastic continua. *International Journal for Numerical Methods in Engineering* 2001; **51**(10):1211–1230.
6. Bui HD. *Inverse Problems in the Mechanics of Materials*: *An Introduction*. CRC Press: Boca Raton, 1994.
7. Lee HS, Kim YH, Park CJ, Park HW. A new spatial regularization scheme for the identification of geometric shapes of inclusions in finite bodies. *International Journal for Numerical Methods in Engineering* 1999; **46**(7):973–992.
8. Yeo IH, Shin S, Lee HS, Chang SP. Statistical damage assessment of framed structures from static responses. *Journal of Engineering Mechanics* (ASCE) 1999; **126**(14):414–421.
9. Park HW. Regularization techniques in system identification for damage assessment of structures. *Ph.D. Thesis*, Seoul National University, Seoul, Korea, 2002.
10. Hjelmstad KD. On the uniqueness of modal parameter estimation. *Journal of Sound and Vibration* 1996; **192**(2):581–598.
11. Hansen PC. *Rank-deficient and Discrete Ill-posed Problems*: *Numerical Aspects of Linear Inversion*. SIAM: Philadelphia, 1988.
12. Groetsch CW. *The Theory of Tikhonov Regularization for Fredholm Equations of the First Kind*. Pitman Advanced Publishing: Boston, 1984.
13. Johnson C. *Numerical Solution of Partial Differential Equations by the Finite Element Methods*. Cambridge University Press: New York, 1987.



DOI: 10.1002/nme

14. Oden JT. *Applied Functional Analysis*: *A First Course for Students of Mechanics and Engineering Science*. Prentice-Hall: Englewood Cliffs, NJ, 1979.
15. Vogel CR. Nonsmooth regularization. In *Inverse problems in Geophysical Application*, Engl HW, Louis AK, Rundell W (eds). SIAM: Philadelphia, 1995.
16. Hansen PC, Mosegaard K. Piecewise polynomial solutions without a priori break points. *Numerical Linear Algebra with Applications* 1996; **3**:513–524.
17. McCormac JC, Nelson JK. *Structural Analysis—A Classical and Matrix Approach* (2nd edn). Addison-Wesley: Reading, MA, 1996.
18. Golub GH, Van Loan CF. *Matrix Computations* (3rd edn). The Johns Hopkins University Press: London, 1996.
19. Barrondale I, Roberts FDK. An improved algorithm for discrete $l_1$ linear approximation. *SIAM Journal on Numerical Analysis* 1973; **10**(5):839–848.
20. Vogel CR. Optimal choice of a truncation level for the truncated SVD solution of linear first kind integral equations when data are noisy. *SIAM Journal on Numerical Analysis* 1986; **23**(1):109–117.
21. Luenberger DG. *Linear and Nonlinear Programming* (2nd edn). Addison-Wesley: Reading, MA, 1989.



DOI: 10.1002/nme